Residence Time and Fluid Mixing on Commercial Scale Sieve Trays

RICHARD L. BELL

Fractionation Research Incorporated, South Pasadena, California

A fiber optic technique was used to obtain point residence time distributions at several points on an 8 ft. diam. sieve tray in hydrocarbon service. Residence time patterns were obtained over a wide range of vapor and liquid loadings with the isopropyl alcohol–water system and at both ends of the cyclohexane toluene system. The data reveal severe flow nonuniformities on the tray including nonuniform velocity distribution and retrograde flow near the column walls. The reasons for this behavior are discussed.

The theoretical calculation of overall Murphree tray efficiency (EMV) from point efficiency (EOG) depends on the specific choice of flow pattern used in the tray model. In 1934 Kirschbaum (*10*) drew attention to the fact that on large trays nonideal flow patterns could exist which would reduce mass transfer efficiency. In 1936 Lewis (*11*) showed that under ideal flow conditions the overall efficiency could greatly exceed point efficiency. The exact nature of ideal and nonideal flow has been the subject of much intensive investigation but a brief discussion of it is appropriate here.

Ideal flow is usually taken to mean the uniform unidirectional movement of fluid from the tray inlet to outlet. Lines of constant residence time would be parallel to the outlet weir for the case of segmental downcomers. Deviations from this behavior can be broadly classified in two categories. In one category would be flow deviations due to velocity gradients across the tray. These gradients could arise from hydraulic imbalances or from flow paths of different lengths due to the tray geometry. In either case a two or three dimensional model for the flow pattern would be required.

The second category of nonideality contains all the various mechanisms which are generally known as turbulent or eddy mixing. It is this second category that has been the focus of virtually every study of tray mixing. Several mechanisms have been proposed for this type of mixing including the splashing model of Johnson and Marangozis (*8*), the pool model of Gatreaux and O'Connell (*6*) and the recirculation models of Warzell (*15*), Oliver and Watson (*13*), and Crozier (*4*). The model which has found the broadest acceptance, however, is the eddy mixing model as it was applied to distillation by Gerster and coworkers (*7*) and incorporated into the AIChE Bubble Tray Design Manual (*1*). Williams and co-workers (*16*) showed that the parameters used in these various models were interrelated and could be expressed in terms of the eddy mixing coefficient.

Because of the difficulties with experimentation on trays in the hazardous environments encountered in industrial operation, nearly all mixing measurements have been conducted in small laboratory columns or simulators. Almost without exception these devices have employed a rectangular geometry and the assumption of uniform, unidirectional flow has been met. As a result a one-dimensional mixing theory (*3*) applied and well-known methods could be used to obtain the mixing parameters.

In general two different tracer techniques, pulse injection and steady state injection, have been used for these experiments and the information from each can be quite different. In the absence of eddy mixing, a residence time experiment (*5*) conducted in a system where velocity profiles exist, will yield results which are indistinguishable from those obtained from eddy mixing alone. If eddy mixing and velocity profiles are both present the residence time distribution will include contributions from both. Unless the flow patterns are known very precisely, it is virtually impossible to separate these effects. On the other hand, the steady state injection experiment (*12*) depends on a net movement of fluid elements upstream from the point of injection. In the absence of reverse or retrograde flow patterns the resultant steady state concentration profiles reflect only the contribution from eddy mixing. It is possible, therefore, that with this technique a velocity distribution could go unobserved.

It is clear that the overall tray efficiency will depend on both types of fluid behavior. Information regarding velocity fields and flow patterns on commercial trays has been extremely limited. Consequently, in order to deal with the problem the assumption of uniform, unidirectional flow with a superimposed mixing component has been used as the basis for current design methods (*1*). The fact that this assumption may be a source of error has been mentioned by several authors (*1, 5, 7*).

R. L. Bell is with the Department of Chemical Engineering, University of California, Davis, California 95616.

TABLE 1. TRAY DESIGN PARAMETERS

Tray type	—Sieve
Tray diameter	—8 ft.
Hole diameter	—½ in.
Hole layout	—1½-in. triangular centers
Hole area	—7.96% of bubbling area
Downcomer	—12.8% of column cross section
Outlet weir length	—75 in.
Outlet weir height	—2 in.
Height under the downcomer	—2 in.
Flow path (inlet to outlet)	—60 in.
No inlet weir or seal pan	

TABLE 2. RANGES OF VARIABLES FOR EACH SYSTEM STUDIED

System	Number of runs	F_s range	Liquid flowrate range (GPM)
Cyclohexane-toluene (C_6 rich)	15	0.573-1.09	51.6-672
Cyclohexane-toluene (Tol rich)	4	0.568-1.09	120-770
Isopropyl alcohol-water	7	0.649-0.793	54.9-489

A relaxation of these assumptions was investigated by Kafarov and co-workers (*17*) where they considered the entrance portion of the tray to be well-mixed and the remainder of the tray to be ideal. This well-mixed portion would correspond to the region of back flow resulting from a hydraulic jump. The effect of several types of flow nonuniformities have been studied by Lebedev and coworkers (*18*) and they predict a marked decrease in efficiency from bypassing due to transverse flow gradients.

In an effort to determine mixing coefficients in commercial scale columns using hydrocarbon systems, Fractionation Research Incorporated (FRI) obtained residence time distributions from the bottom of successive downcomers in a 4 ft. diameter column (*14*). These data contained the cumulative effect of downcomer and tray mixing which unfortunately could not be separated. Analysis of the data, however, suggested indirectly that severe flow nonuniformities were present. To obtain data from the tray alone and to detect any nonuniformities that were present, a fiber optic technique for measuring point residence time distributions (RTD's) on an operating commercial scale tray was employed. The results from an 8-ft. diam. sieve tray are reported in this paper.

EXPERIMENTAL METHOD

The complete details of the fiber optic method have been reported in a previous paper (2). The basic schema of the method is illustrated in Figure 1. A 250 cc. volume of 0.59 g./liter solution of fluorescein dye, (Yellow C-4, Patent Chemicals Corp.) was rapidly injected into the top downcomer of the column. As the tracer passed the tip of the bifurcated fiber optic probes installed on the second tray from the top, it was excited by the filtered light carried from the mercury arc lamp by one limb of the probe bifurcation. A portion of the resultant fluorescence was transmitted through the second limb of the bifurcation, through a filter to a photomultiplier tube. As discussed in (2), the output of the photomultiplier tube is directly proportional to the local tracer concentration in the range of tracer concentration used. The resultant RTD's were digitized and logged for later calculation of first and second moments.

The design parameters of the tray tested are given in Table 1. The probes were installed in a rectangular array on one-half of the tray and in the geometric center of the following downcomer as shown in Figure 2. The trays were installed level using standard FRI installation procedures.

EXPERIMENTAL RESULTS

Data were obtained from 3 systems; cyclohexane-toluene (toluene rich), cyclohexane-toluene (cyclohexane rich) and isopropyl alcohol-water. Table 2 gives the ranges of variables studied for each system.

Each run was replicated at least 4 times. In nearly all runs the individual replicates were smooth and highly reproducible and two methods were used to obtain the

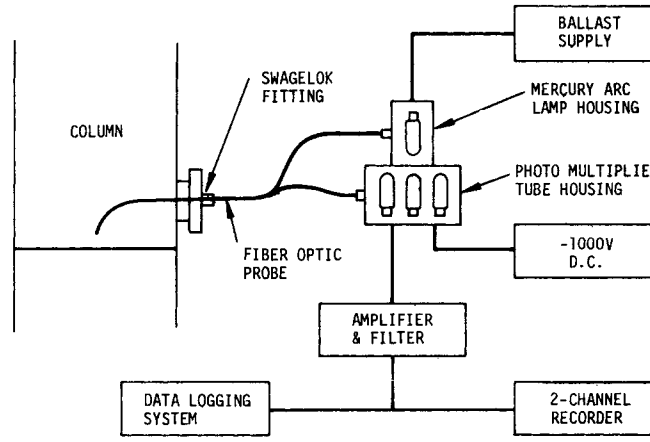

Fig. 1. Schematic diagram of fiber optic system.

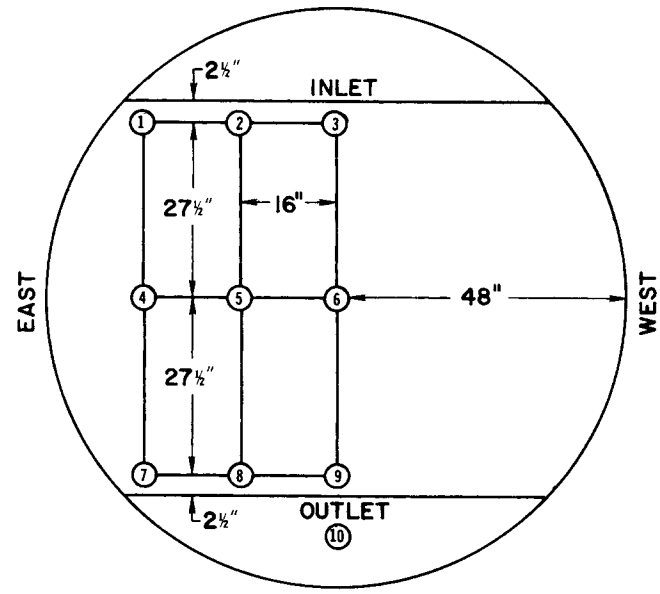

⑥ = Position Number

Fig. 2. Fiber optic probe layout on the tray.

TABLE 3. COMPARISON OF REPLICATES RUN NUMBER 9712 DYE SHOT NUMBER 3 ON MARCH 27-28, 1969
Replicates Corrected for Input Synchronization

First Moments (sec.)

Position	Replicate number 1	2	3	4	Avg.	Std. dev.	0/0 dev.
1	62.91	65.68	63.36	61.15	63.28	1.86	2.94
2	64.27	68.13	64.84	65.65	65.72	1.70	2.59
3	60.36	61.64	61.03	59.05	60.52	1.11	1.83
4	86.89	87.96	87.90	87.18	87.48	0.53	0.61
5	84.80	82.12	84.22	83.45	83.65	1.16	1.38
6	68.56	68.45	70.08	66.56	68.41	1.43	2.10
7	85.33	83.74	85.07	84.98	84.78	0.70	0.83
8	75.71	74.36	74.91	76.46	75.36	0.91	1.21
9	72.75	71.20	70.98	76.19	72.78	2.40	3.30
10	83.10	81.40	82.29	84.01	82.70	1.11	1.34
AVG.	71.78	73.05	75.01	78.03			
°COR.	2.68	1.42	−0.54	−3.56			
AVG. OF COLUMN AVERAGES			74.47				

Second Central Moments (sec.°° 2)

Position	Replicate number 1	2	3	4	Avg.	Std. dev.	0/0 dev.
1	874.89	974.02	862.87	907.20	904.74	49.83	5.50
2	1040.76	1198.46	1005.92	1350.80	1148.98	158.48	13.79
3	801.66	863.23	849.62	837.54	838.01	26.40	3.15
4	1267.58	1309.89	1265.18	1357.60	1300.06	43.50	3.34
5	1418.09	1062.99	1184.71	1447.66	1278.36	185.59	14.51
6	967.97	1020.54	1184.80	796.94	992.56	159.80	16.09
7	1188.50	1164.16	1258.70	1091.35	1175.68	69.04	5.87
8	1100.22	1106.55	1090.39	1017.17	1078.58	41.47	3.84
9	1010.17	1008.40	967.51	1061.25	1011.83	38.38	3.79
10	1271.13	1232.74	1271.27	1073.45	1212.14	94.22	7.77
AVG.	1046.43	1046.67	1114.74	1168.54			
°COR.	47.67	47.42	−20.64	−74.44			
AVG. OF COLUMN AVERAGES			1094.10				

° Avg. of the column − avg. of column averages.

first and second moments of the RTD.° The first method was to calculate the moments for each replicate and average the results. From this calculation an estimate of the standard error for the data from a given run was obtained. The second method was to use the method of average transients in which the replicates were added point by point to eliminate low frequency noise (2). When there was an excessive low frequency noise component on each replicate only the method of average transients was used. In a very small number of cases it was necessary to further smooth the data by averaging 3 adjacent data points to eliminate severe noise. An exponential fit of the tail region was used to extrapolate the data to infinity. Moments were obtained by integration of the RTD to infinite time. This was done by numerically integrating the experimental data to the tail region where an analytic integration based on the exponential decay assumption was used.

Tables 3 and 4 contain typical calculation summary sheets. Table 3 shows the individual replicates for run 9712 (C_6-toluene (toluene rich) $F_s = 0.573$ GPM = 112). The data from each of the 10 points on the tray were averaged and the individual replicates synchronized so these averages would coincide. This corrected for time delays during pulse injection. The averages for the replicates, the standard deviations and the percent deviations were tabulated. Table 4 compares the results obtained by averaging the replicates with the results obtained by summing the replicates to obtain a single smooth curve. The calculation summary sheets together with the run conditions for each run are on file with the American Documentation Institute.

The average % standard deviation between replicates was 1.84% for the mean residence times and 11.2% for the second central moments.° The % difference between the values for both moments, obtained by treating the replicates individually or by the method of average transients, was typically 0.5%.

Lines of constant residence time were obtained by cross plotting the data from the 9 probes on the tray. A set of typical cross plot curves is shown in Figure 3 and the tray profile derived from them is shown in the first of the three profiles in Figure 4. The profiles for the cyclohexane rich end of the system are virtual reproductions of those in Figure 4 indicating that the observed behavior was characteristic of the tray. Miniature profiles showing the general characteristics of the residence time patterns as a function of F_s and flowrate are shown for the cyclohexane-toluene (toluene rich) system in Figure 5 and for the IPA-water system in Figure 6. The data for the cyclohexane-toluene (cyclohexane rich) system are almost identical to that for the toluene rich system shown in Figure 5. Lines of con-

° See Notation for definition of moments.

° See Notation for definition of % standard deviation and second central moment.

TABLE 4. COMPARISON OF REPLICATE AVERAGES AND SUMMED DATA RUN NUMBER 9712 DYE SHOT NUMBER 3 ON MARCH 27-28, 1969

Replicates Corrected for Input Synchronization
First Moments (sec.)

Position	Summed data	Avg. of reps.	0/0 diff.
1	63.37	63.28	0.15
2	65.87	65.72	0.21
3	60.69	60.52	0.27
4	87.48	87.48	0.00
5	83.37	83.65	0.32
6	68.23	68.41	0.26
7	84.80	84.78	0.02
8	75.45	75.36	0.11
9	72.98	72.78	0.28
10	82.80	82.70	0.11

Second Central Moments (sec.** 2)

Position	Summed data	Avg. of reps.	0/0 diff.
1	910.69	904.74	0.65
2	1154.98	1148.98	0.52
3	848.80	838.01	1.28
4	1296.64	1300.06	0.26
5	1238.74	1278.36	3.09
6	967.50	992.56	2.52
7	1179.96	1175.68	0.36
8	1091.08	1078.58	1.15
9	1029.42	1011.83	1.73
10	1219.78	1212.14	0.62

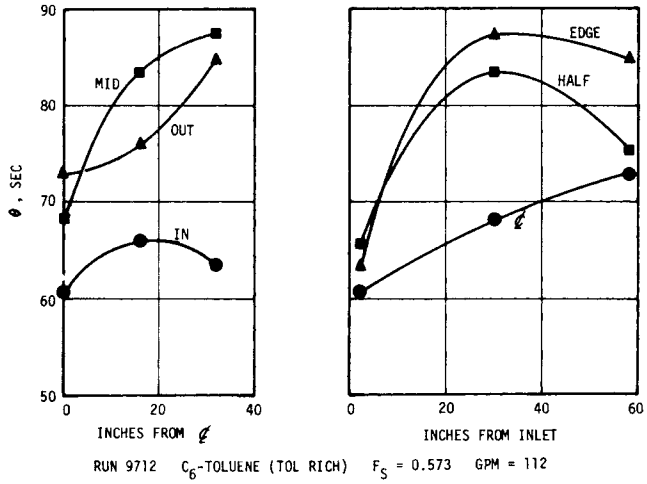

Fig. 3. Typical cross plots of residence time data.

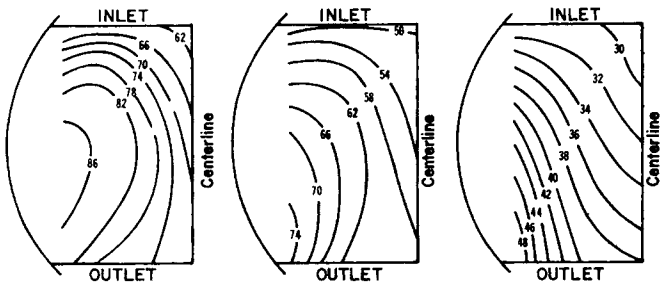

a. Run 9712, F_S = 0.573, GPM = 112 b. Run 9713, F_S = 0.836, GPM = 160 c. Run 9714, F_S = 1.04, GPM = 202

Fig. 4. Residence time profiles for the cyclohexane-toluene system (toluene rich) on a sieve tray operating at total reflux.

stant second central moment were obtained in a similar fashion and showed characteristics very similar to the residence time profiles. The second central moment profiles corresponding to the residence time profiles in Figure 4 are shown in Figure 7.

The distinctive feature of these profiles is the zone of extended residence time near the wall and the relatively shorter residence time near the centerline. This result is in striking contrast to the profiles which would be expected if the assumptions of the current theory applied. This is particularly evident at low liquid and gas loads where an actual "pooling" of liquid seems to occur. As both the liquid and gas rates are increased the nonideality is reduced but not completely eliminated. At the highest liquid and gas rates even though there continues to be longer residence time at the wall, the lines of constant residence time are becoming more nearly parallel and the "pooling" tendency is eliminated. This suggests that since the lines are parallel the flow is unidirectional although a velocity

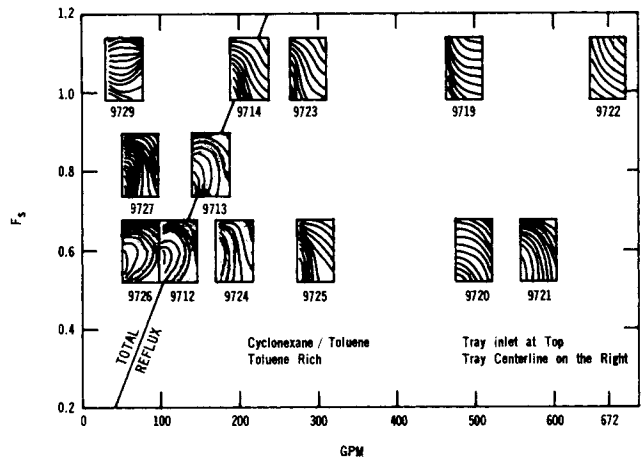

Fig. 5. Residence time profiles as a function of F_S (gas flowrate factor) and GPM for the cyclohexane-toluene system on an 8-ft. diam. sieve tray.

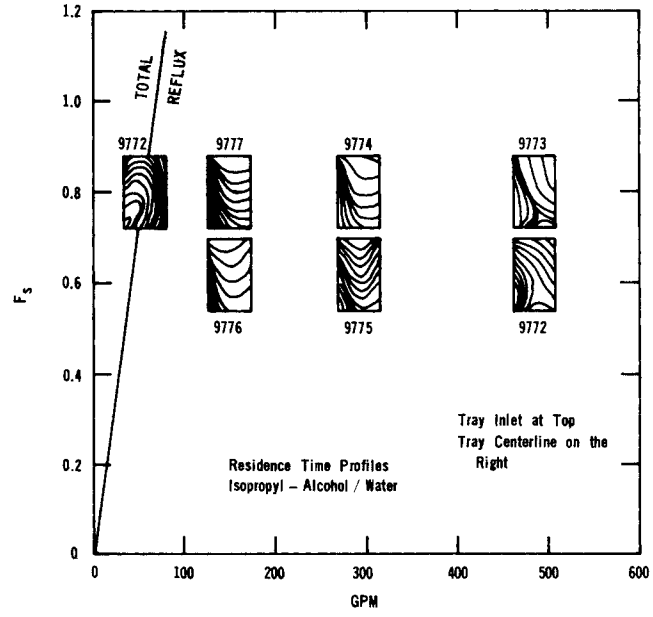

Fig. 6. Residence time profiles as a function of F_S (gas flowrate factor) and GPM for the isopropyl alcohol-water system on an 8-ft. diam. sieve tray.

profile still exists. The effect of two dimensional eddy mixing in this case will be to obscure the precise details of the velocity distribution. Possible reasons for this behavior will be discussed later.

As shown in Figures 4, 5, and 6, the lines of constant residence time were not necessarily parallel to the inlet. This raised the question as to whether the profiles were the result of action on the tray or were established in the downcomer or perhaps by a cumulative tray to tray effect. The fact that the most severe conditions existed at low vapor loads suggested that no generality would be sacrificed if this point were studied by water table experiments. As it turned out the most severe conditions are realized with no vapor flow.

For these experiments the entire active area of the test tray in the 8-ft. diam. column was blanked. The tray geometry and dimensions remained as shown in Table 1. Three probes were installed in the downcomer and 13 on the tray. The residence time profiles on the tray were very similar to those presented in Figure 4. The most important

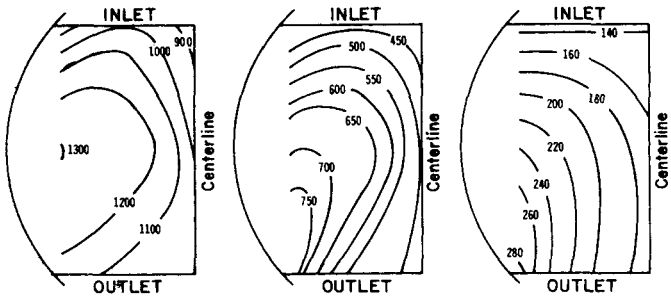

a. Run 9712, $F_S = 0.573$, GPM = 112 b. Run 9713, $F_S = 0.836$, GPM = 160 c. Run 9714, $F_S = 1.04$, GPM = 202

Fig. 7. Lines of constant second central moment of the RTD for the cyclohexane-toluene system (toluene rich) on 8-ft. diam. sieve trays operating at total reflux.

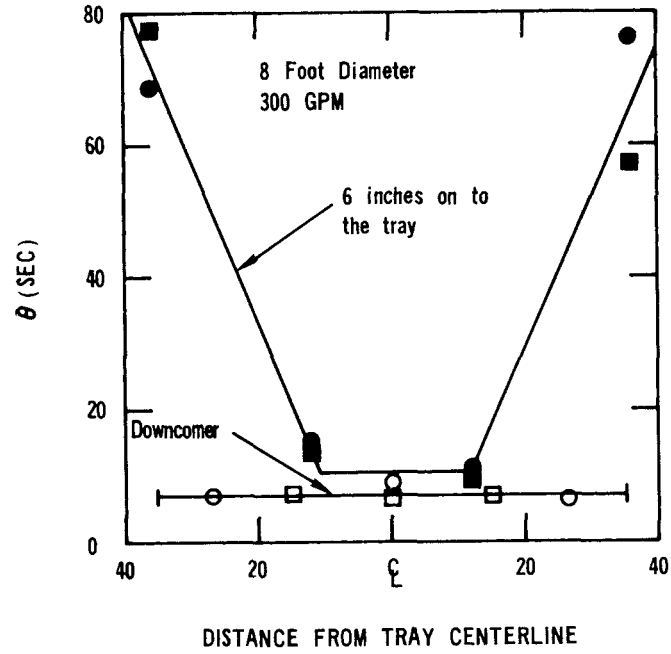

Fig. 8. Plot of residence time in the downcomer and 6 in. from the downcomer apron onto the tray.

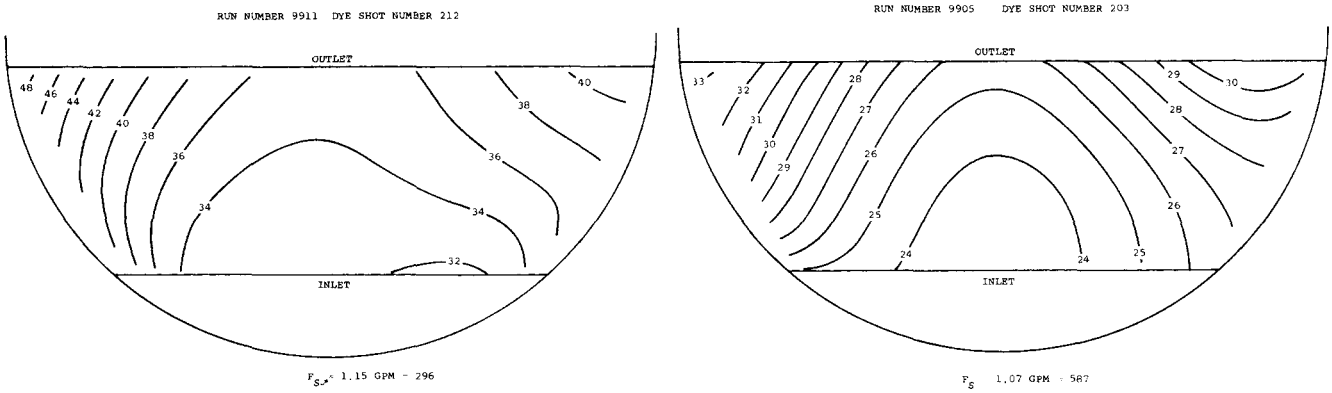

Fig. 9. Residence time profiles on a split flow 8 ft. diam. tray. Flow is from side to center for the cyclohexane-toluene system.

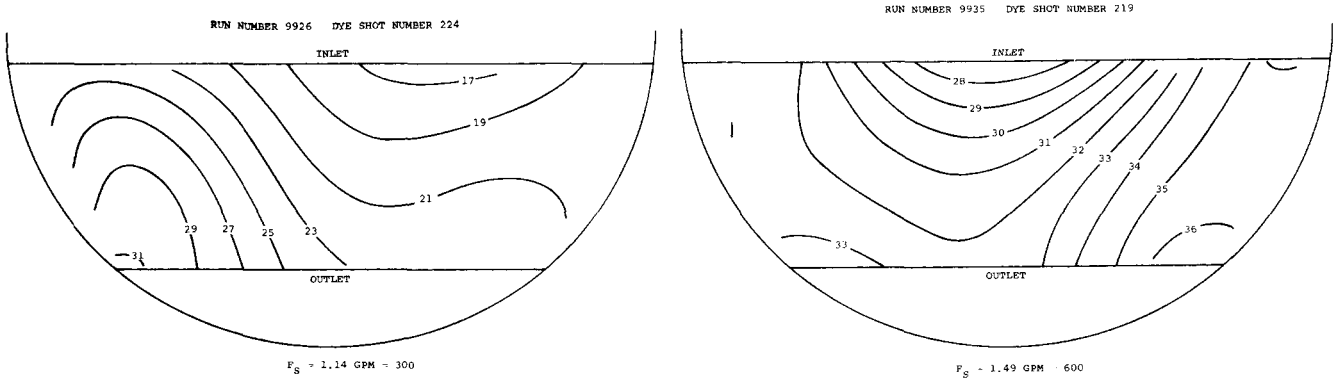

Fig. 10. Residence time profiles on a split flow 8 ft. diam. tray. Flow is from center to side for the cyclohexane toluene system.

observation, however, was that the residence times measured at the bottom of the downcomer were constant. The significance of this finding is best illustrated by the data shown in Figure 8 which are typical of the data obtained over the range of 150 GPM to 500 GPM. In the upper portion of the figure the data from the set of probes located 6 in. from the inlet are plotted. In the lower portion the data from the probes in the downcomer are plotted. The experiment was repeated several days later to obtain a wider spacing of the downcomer probes. The two sets of data are indicated by squares and dots. There is no question that the residence time pattern seen 6 in. onto the tray could not have come from a pattern established in the downcomer. The profiles which were measured are therefore the result of events which occur after the liquid enters the tray.

In large diameter towers, multipass trays are sometimes used to obtain more uniform distribution of liquid. Residence time data were obtained from a two-pass tray in the 8-ft. tower. Typical profiles for the side-to-center, and center-to-side patterns are shown in Figures 9 and 10. Here again flow nonuniformities are in clear evidence.

LIQUID CIRCULATION ON THE TRAY

Although data were not obtained next to the column wall, a simple extrapolation of the profiles in Figure 4 will yield lines of constant residence time which are closed. The flow patterns which produce these profiles must be complex. A simple potential flow explanation would require the fluid to be pouring from the tray through a hole at the center of the profile closure. This is clearly not the case. The alternate explanation is a high speed flow down the center of the tray with retrograde flow near the wall.

The presence of retrograde flow near the wall has been conclusively demonstrated by two sets of experiments. In the first a pulse of dye was injected at the centerline of an active tray. In Figure 11 the normalized distributions obtained from 6 probes placed in a regular rectangular pattern on half the tray are reproduced. The pulse can be followed from the inlet (probe 3), across the tray to the outlet (probe 9). It then appears at the outlet corner (probe 7) and can be followed back down the tray to the

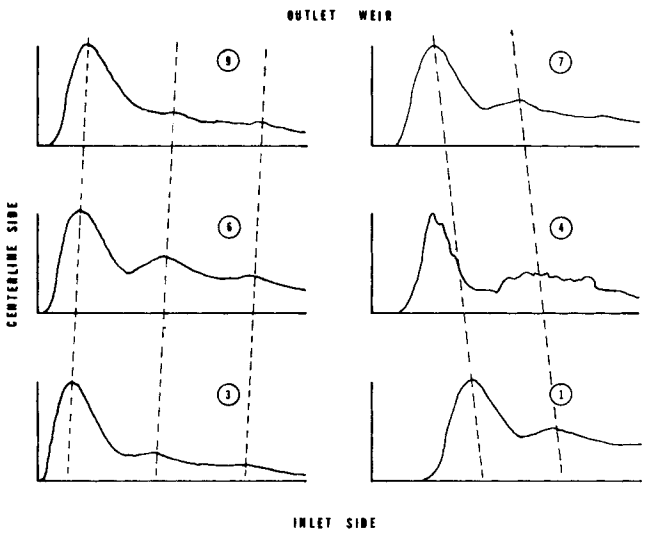

Fig. 11. Recurrent peaks resulting from a single pulse input at the inlet centerline of the tray. For the exact position of the probes see Figure 2 (numbers correspond to position number).

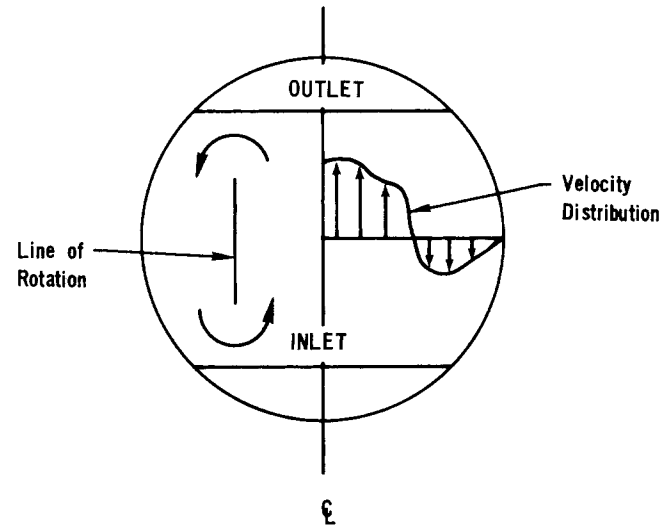

Fig. 12. Typical velocity distribution on the tray.

inlet corner (probe 1). The major peak from probe 1 then appears as the secondary peak moving down the centerline again. The location of the probes was the same as shown previously in Figure 2. In all, three passes around the tray can be identified. The slope of the dashed lines through the peaks yield a measure of the velocity, since the probes were equally spaced across the tray. Comparing the slopes shows that the velocity down the centerline was more than twice the velocity near the wall. The reason for the distorted profile at probe 4 was made clear during the flow visualization experiments.

Although the tray residence time profiles together with the data shown in Figure 11 gave compelling evidence that there was a circulating pattern on the tray, visual observation of the tray being tested or of motion pictures of other active trays failed to yield any visual evidence that these patterns existed. To see if these patterns could be visualized, an 11-cm. water table simulator with a downcomer geometry the same as on the 8-ft. tray, was constructed. A dye tracer clearly showed the high speed centerline flow and the retrograde flow at the wall that appeared to exist on the larger tray. Again, without the tracer there was no visual indication that such a pattern existed. To study scale up effects a 4-ft. diam. simulator was constructed which duplicated the 4 ft. tower geometry. An extensive series of flow visualization experiments again showed the presence of retrograde flow. The fluid on the tray rotated about a line of rotation located symmetrically in either side of the centerline. The location of the lines of rotation changed only slightly over a wide range of flow rates and did not depend on wall curvature. A film summarizing these experiments together with subsequent column experiments has been presented by Keller and Yanagi (9).

On the basis of these results it now seems quite clear that at least over some range of liquid and gas loads a velocity profile exists which can be schematically represented as shown in Figure 12. The distortion occurring at point 4 in Figure 11 was due to the fact the probe was located almost exactly on the line of rotation.

FACTORS CAUSING RETROGRADE FLOW

The reasons for this circulation and ways of correcting it are still under study, but at this time there are at least 3

factors which have been identified: 1. nonuniform pressure distribution at the tray inlet, 2. stagnation at the outlet weir, and 3. flow separation because of the jetting action at the center of the inlet. Their relative contribution depends on the flowrates of liquid and vapor as well as tray geometry. The presence of tray hardware will also influence or entirely change their effect.

Of the three reasons suggested, the most important seems to be the nonuniform pressure distribution at the inlet. This is caused by the focusing effect of the curved wall of the segmental downcomer. The effect of the curvature is to direct the liquid coming over the weir toward the center of the inlet of the tray below. The result is a nonuniform pressure distribution due to loss of velocity head, causing a high volumetric flowrate under the central portion of the downcomer apron. On the tray this results in a relatively high velocity flow down the central portion of the tray. As the downcomer fills up with clear liquid or froth the tendency will be to distribute the pressure more uniformly.

Second in importance is the effect of stagnation at the outlet weir. At the stagnation point the liquid is forced laterally to either side of the centerline as well as over the weir. With the hydraulic imbalance present at the tray inlet the flow component parallel to the weir drives the fluid in the reverse direction near the wall. In some simulator studies the retrograde circulation pattern extended under the downcomer apron and into the downcomer itself.

Finally the presence of the high velocity centerline flow can under certain conditions cause flow separation. The adverse pressure gradient caused by the separation acts to increase the retrograde motion. Flow separation will be more likely to occur with shorter downcomers.

The simulator studies showed that a delicate hydraulic balance was present and that relatively small causes could produce large effects. In particular the effect of reducing the pressure nonuniformity at the tray inlet was very important. This can be seen in Figure 6. As the liquid load increases the downcomer backup tends to increase and the pressure is more uniformly distributed. This causes a stronger component of flow near the wall and overcomes the retrograde velocity component due to stagnation.

MIXING

In addition to the velocity gradients there must be an eddy mixing component due to agitation by the vapor. In the one dimensional theories for calculating mixing coefficients from residence time data, the change in variance of the RTD is measured for fluid elements moving directly from say point A to point B on the tray. Because the flow is unidirectional with uniform velocity, and since no gradients in tracer concentration are considered except in the direction of flow, there can be no influence at point B except from fluid that passed point A. In the experiments presented in this paper, the RTD measured at point B may be the resultant of contributions from many points on the tray due to velocity and mixing effects. There is no simple theory which will allow direct calculation of mixing coefficients from this type of data. This is best illustrated by reference to the point equation which could be used to describe this situation.

$$\frac{\partial C}{\partial \theta} = \underset{\sim}{q} \cdot \nabla C - \nabla \cdot (\underset{\approx}{Pe^{-1}}) \cdot \nabla C \qquad (1)$$

Term $\underset{\sim}{q}$ is a dimensionless velocity distribution which has been normalized by the mean velocity which would exist if the flow were ideal. The term $(\underset{\approx}{Pe^{-1}})$ denotes the two (or three) dimensional dependence of the eddy mixing coefficient as contained in the Peclet number. Numerical techniques are required for the solution of Equation (1) for arbitrary velocity and mixing profiles. Residence time and second moment profiles similar to those presented in Figure 4 are being obtained from the numerical solution of Equation (1). The computed profiles will then be compared to the measured distributions to obtain specific velocity and mixing patterns. These results will be presented in a subsequent paper.

EFFECT ON MASS TRANSFER

The ultimate values of these findings lies not in the discovery of nonuniform flow patterns but the effect that these patterns have on tray efficiency. It has been shown that these patterns exist over a wide range of operating variables which include those used in typical sieve tray applications. As a result it must be considered that such patterns are characteristic of sieve trays. The present methods of obtaining the efficiency of these trays does not account for this effect, and consequently it would be fortuitous if the method gave accurate predictions.

It is not known at this time to what extent the efficiency is affected if at all. However, measurements of liquid composition on the tray yield composition profiles such as that shown in Figure 13. Here again the effect of long residence time near the wall and the tendency for "pooling" can be seen. The high velocity and the resultant high volumetric flow down the centerline in essence causes the liquid to bypass the tray. This should result in a reduction of efficiency. Preliminary results from the numerical integration of the general transport equation [Equation (2)] show

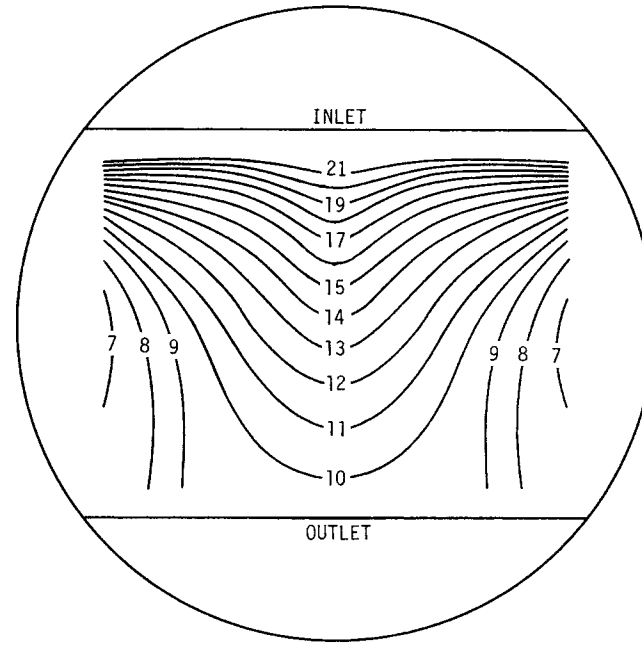

RUN 9708 - 8 FT COLUMN

Fig. 13. Lines of constant composition obtained from a tray operating with a nonuniform velocity distribution.

that for unidirectional flow with a velocity profile the tray efficiency is always less than that predicted for the uniform velocity distribution.

$$0 = \underset{\sim}{q} \cdot \nabla C - \nabla \cdot (\underset{\approx}{Pe}^{-1}) \cdot \nabla C + \lambda EO_G (C^* - C) \tag{2}$$

Referring to Equation (2) it can be seen the important parameters are λ, EOG, $\underset{\approx}{Pe}$, and $\underset{\sim}{q}$. The preliminary results show that for low values of λEOG the effect is small.

CONCLUSIONS

The fiber optic method for measuring point RTD's has been successfully used to obtain residence time distributions on a large diameter sieve tray under commercial operating conditions.

The results of the residence time studies together with information from simulator studies have conclusively demonstrated the presence of circulating flow patterns with a retrograde component near the wall. These patterns are characteristic of sieve trays and exist over a wide range of operating variables. It is impossible at this time to compute velocity profiles or mixing coefficients directly from the residence time data. The composition profiles obtained from these trays are also two dimensional and show many of the characteristics of the residence time profiles.

It is clear that the assumptions of current tray efficiency prediction methods are not being met. The flow nonuniformities are a source of inefficiency which is not accounted for but there is much work yet to be done before their full effect on tray efficiency is known. The results presented in this paper provide insight into the exact nature of flow patterns to be used in future models. If it is shown that the efficiency of a tray is substantially reduced then the approach should be not to design for the inefficiency but instead to correct it.

ACKNOWLEDGMENT

The author gratefully acknowledges the invaluable advice and assistance of George J. Keller, Gautam B. Shah, and Tak Yanagi, all of FRI, in obtaining and analyzing the results reported in this paper.

NOTATION

C = concentration at a point on a tray
C^* = liquid concentration in equilibrium with incoming vapor
EOG = Murphree point efficiency
EMV = Murphree tray efficiency
F_s = $V_s \rho_v^{1/2}$ V_s is superficial vapor velocity and ρ_v is the gas density
$f(t)$ = residence time distribution used in definition of moments
$\underset{\approx}{Pe}$ = Peclet number denoting three dimensional eddy mixing
q = normalized velocity profile
RTD = residence time distribution
$\bar{t}$ = residence time taken to be equal to the first moment of the RTD
x_i = value of i^{th} replicate
$\bar{x}$ = average value of all replicates
λ = stripping factor mG/L
θ = dimensionless time

$$\text{First moment} = \frac{\int_0^\infty t\, f(t)\, dt}{\int_0^\infty f(t)\, dt} = \bar{t} \text{ (mean residence time)}$$

$$\text{Second moment} = \frac{\int_0^\infty t^2 f(t)\, dt}{\int_0^\infty f(t)\, dt}$$

$$\text{Second central moment} = \frac{\int_0^\infty (t - \bar{t})^2 f(t)\, dt}{\int_0^\infty f(t)\, dt}$$

$$\text{Standard deviations} = \left[\frac{\sum_{i=1}^{N} (x_i - \bar{x})^2}{N - 1} \right]^{1/2} = \text{S.D.}$$

$$\% \text{ standard deviation} = \frac{\text{S.D.}}{\bar{x}} \times 100$$

LITERATURE CITED

1. "Bubble Tray Design Manual; Prediction of Fractionation Efficiency," Am. Inst. Chem. Engrs., New York (1958).
2. Bell, R. L., *AIChE J.*, **18**, 491 (1972).
3. Bischoff, K. B., O. Levenspiel, *Chem. Eng. Sci.*, **17**, 257 (1962).
4. Crozier, R. S.; Ph.D. thesis, Univ. of Mich., Ann Arbor (1956).
5. Foss, A. S., J. A. Gerster, R. L. Pigford, *AIChE J.*, **4**, 231 (1958).
6. Gatreaux, M. F., N. E. O'Connell, *Chem. Eng. Progr.*, **51**, 232 (1955).
7. Gerster, J. A., A. B. Hill, N. N. Hochgraf, D. B. Robinson, *Tray Efficiencies in Distillation Columns Final Report*, Univ. of Delaware, Newark (1958).
8. Johnson, A. I., J. Marangozis, *Can. J. Chem. Eng.*, 161 (1958).
9. Keller, G. J., T. Yanagi, Film presented at 68th National Meeting Am. Inst. Chem. Engrs. (1970).
10. Kirschbaum, E., *Distillation and Rectification*, Chemical Publ. Co., Brooklyn, N. Y. (1948).
11. Lewis, W. K., Jr., *Ind. Eng. Chem.*, **28**, 399 (1936).
12. Miyauchi, T., I. Hiroshi, K. Kuba, *Kugaku Kogaku*, **5**, 20 (1967).
13. Oliver, E. D., C. D. Watson, *AIChE J.*, **2**, 18 (1956).
14. Sakata, M., *Chem. Eng. Progr.*, **62**, 98 (1966).
15. Warzell, Ph.D. thesis, Univ. of Mich., Ann Arbor (1955).
16. Williams, B., J. W. Begley, C. H. Wu, *Tray Efficiencies in Distillation Columns, Final Report*, Univ. of Mich. (1960).
17. Kafarov, V. V., V. V. Shestopalov, B. M. Gorenshtein, Theoret. Osnovy Khim. Teknol., **2**, 628 (1968).
18. Lebedev, Y. N., I. A. Aleksondorov, D. D. Zykov, *ibid.*, 183 (1968).

[*] Supplementary data has been deposited as Document No. 01719 with the National Auxiliary Publications Service (NAPS), c/o CCM Information Corp., 866 Third Ave., New York 10022 and may be obtained for $4.00 for microfiche or $11.60 for photocopies.

Manuscript received April 6, 1971; revision received November 22, 1971; paper accepted November 22, 1971.